Chapter 4

EFFECT OF FABRIC ON SHEAR WAVE VELOCITY IN GRANULAR MATERIALS

[1] U. Mital, R.Y. Kawamoto, and J.E. Andrade. "Effect of fabric on shear wave velocity in granular materials". submitted. 2016.

4.1 Introduction

The small-strain elastic shear wave velocity (V_S) is a basic mechanical property of soils and is an important parameter in geotechnical engineering. Together with the results of standard and cone penetration tests, it helps model the response of geomaterials to dynamic loading processes such as earthquakes and vibrations. Recently, V_S has been adopted as one of the indices (in addition to penetration resistance) for development of liquefaction charts [5, 34, 88]. Liquefaction charts are developed using the "simplified procedure" and are used to evaluate liquefaction resistance of soils in earthquake-prone regions [71].

The use of V_S as an index to quantify liquefaction resistance is based on the fact that both V_S and liquefaction resistance are similarly affected by many of the same parameters (such as void ratio, stress state, stress history and geologic age) [5]. Therefore, an understanding of how such parameters affect V_S helps in understanding the effect of such parameters on liquefaction resistance of soils. For instance, the effect of parameters such as relative density, stress state, and geologic age on soil resistance indices such as V_S are accounted for, and consequently their effects are incorporated in the evaluation of liquefaction resistance [34, 88]. Another important parameter whose effect is widely acknowledged to have a significant influence on liquefaction resistance is grain arrangement, or fabric [34]. Experiments have shown that the method of sample preparation, or the depositional environment, can significantly affect soil fabric and cause soils with the same stress states and relative densities to behave differently [46, 47, 62]. In fact, the effect of fabric has been established as a major concern when it comes to testing field samples in the laboratory, on account of sampling disturbance destroying the grain fabric. Quantification of in-situ fabric is still an open problem, and hence considerable judgement is needed in order to map laboratory test results to field conditions.

Given the effect of fabric on liquefaction resistance, it seems reasonable to expect that fabric also affects V_S. Indeed, Stokoe et al [75] proposed empirical correlations relating V_S to confining stresses where the proportionality constant is believed to be a function of soil fabric. Micro-mechanical studies have also been conducted that explore the effect of soil structure or fabric on small-strain shear modulus $G_{\max}$, which is proportional to V_S [1, 63, 89]. Such studies are important in order to quantify the effect of fabric while assessing liquefaction resistance.

In this paper, we conduct numerical simulations to investigate the effect of fabric on shear wave velocity (V_S) of soils. We use the 'level set discrete element method' (LS-DEM) [39, 41] and show that two granular assemblies, with the same stress state and void ratio but different fabric, can exhibit different liquefaction behavior. Subsequently, via a numerical implementation of the bender element test [49, 64, 74], we also obtain different V_S estimates for the two assemblies. Our results suggest how fabric can affect both liquefaction behavior and V_S of a granular assembly, suggesting that V_S can act as a proxy to account for the fabric effect while evaluating liquefaction resistance. We observe a possible correlation between fabric anisotropy and V_S anisotropy, quantification of which could imply that a knowledge of V_S anisotropy in the field would give us insight regarding the micro-mechanical structure of in-situ soil. For laboratory testing or simulation of soils, this could help in selection or development of a sample preparation technique that yields a similar V_S anisotropy as that in the field. Furthermore, a comparison of in-situ fabric and laboratory fabric could aid researchers in more accurately mapping laboratory or simulation results to field conditions.

4.2 Simulation Methodology

Our numerical investigation was conducted using the 'level set discrete element method' (LS-DEM) [39, 41]. LS-DEM is a variant of the discrete element method (DEM), which is a numerical method that describes the mechanics of an assembly of particles [17]. LS-DEM enables an accurate depiction of irregular particle shapes using level sets. In this work, we used a 2D level set representation of caicos ooid grains as obtained by Lim et al [52], following the characterization methodology proposed by Vlahinic et al [83]. The caicos ooid grains were obtained in dimensions of pixels. These were rescaled assuming a pixel size of 0.1095^2 mm^2, yielding a

mean grain area of 5.4 mm^2. Thickness of grains was assumed to be 1 pixel length. Table 4.1 outlines the values of model parameters used in the LS-DEM model. Our time step was equal to 1.36 μs, which is smaller than the critical time step required for stable DEM analysis [77].

Table 4.1: Model parameters and values used in the LSDEM model

Model parameters	Values
Inter-particle friction	0.3
Wall friction	0
Normal contact stiffness (Particle and wall)	2.74×10^8 N/m
Particle shear contact stiffness	2.47×10^8 N/m
Particle density	2.7×10^3 kg/m^3
Global damping	5×10^3 s^{-1}
Contact damping	0
Time step	1.36×10^{-6} s

Fabric quantification

We quantified fabric using the classic 2nd order fabric tensor based on contact normals [40]:

$$F_{ij} = \frac{1}{N} \sum_{c=1}^{N} n_i^c n_j^c \tag{4.1}$$

where n_i^c is the $i-$th component of contact normal at contact c. The fabric anisotropy A is defined as:

$$A = 2(F_1 - F_2) \tag{4.2}$$

where F_1 and F_2 are the major and minor principal values, respectively, of the fabric tensor. The orientation (θ_F) of F_1 may be used to define the orientation of fabric anisotropy A. We can use a 2nd order Fourier expansion to obtain the probability density $P(\theta)$ of contact normals [12]:

$$P(\theta) = \frac{1}{2\pi}\{1 + A\cos 2(\theta - \theta_F)\} \tag{4.3}$$

where θ is the orientation of a contact normal. A perfectly isotropic fabric will be circular in polar coordinates, whereas an anisotropic fabric will tend towards a 'peanut' shape.

There are many different ways to quantify fabric. Kuhn et al [45] provides a good review. The anisotropic stiffness of a granular assembly is inherently linked to the

directionality of force chains. Therefore, choosing contact normals as a basis for fabric quantification seems justified.

Granular assembly generation

Our objective here was to obtain two granular assemblies with similar stress states and void ratio but different fabric. Figure 4.1 summarizes our methodology to obtain an initial assembly. Computational limitations necessitated the use of an unconventional approach to assembly generation. An initial assembly of 800 grains was first developed (explained below) which was duplicated and placed in a 2x2 grid, resulting in 3200 grains. This resulted in clear interfaces visible at the boundaries of the individual 800 grain assemblies. To remove the interfaces, the assembly was first isotropically consolidated to 100 kPa, then a central bin of grains was perturbed at an angle of 45 degrees. The inter-particle friction was then temporarily turned off, and the assembly allowed to relax, resulting in a stress-free assembly with grains densely packed together. The inter-particle friction was turned back on and the assembly was isotropically consolidated to 100 kPa.

To obtain the 800 grain assembly, grains were placed in a hexagonal packing such that no two particles were in contact with each other. The aspect ratio of the packing was approximately 1:2, with the approximate dimensions being 5 cm $\times$ 10 cm. The assembly was then isotropically consolidated to 5 MPa, then unloaded to 100 kPa, and then subjected to constant volume biaxial loading to change the aspect ratio to 1:1. The resultant assembly had a predominantly vertical fabric (not shown). The inter-particle friction was then temporarily turned off, and the assembly allowed to relax, resulting in a stress-free assembly with grains densely packed together. This assembly was then duplicated to generate the 3200 grain assembly (as described above).

The resultant 3200 grain assembly, isotropically consolidated to 100 kPa, was then subjected to two different loading histories, in order to generate two assemblies with similar stress states and void ratio, but different fabric anisotropy. The initial fabric of the assembly is shown in Figure 4.2. We refer to the two assemblies as ‘assembly 1’ and ‘assembly 2’. The loading history for assembly 1 involved simple shear loading, sheared to an angle of 20 degrees, and subsequently sheared back to 0 degrees. This gave the assembly a pronounced diagonal anisotropy (Figure 4.2),

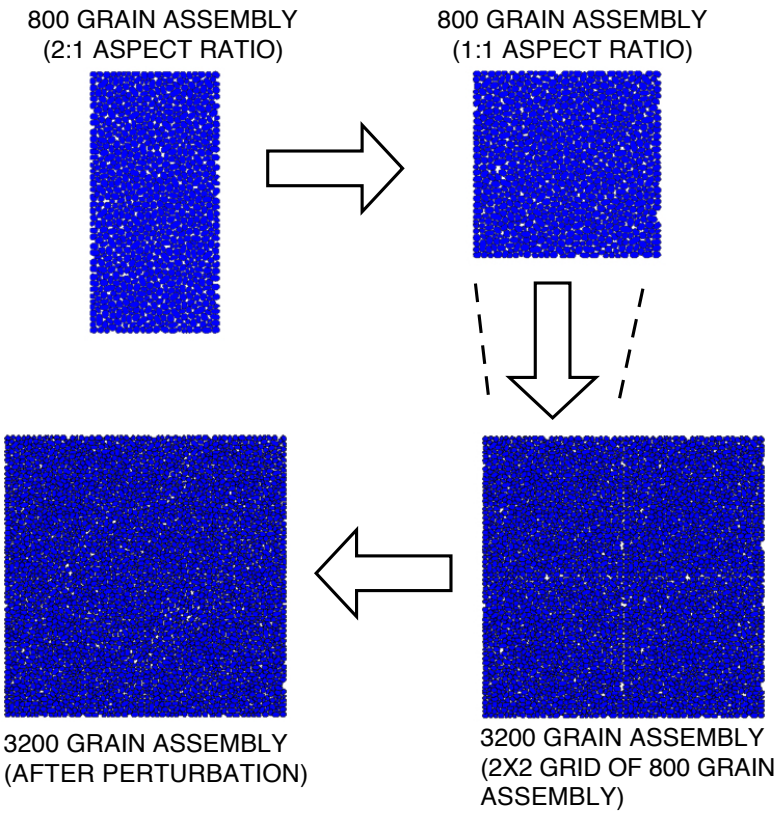

Figure 4.1: Initial assembly generation

with the fabric oriented at an angle of 34 degrees clockwise with the vertical. The assembly had a resultant void ratio of $e = 0.17$, and a stress state of $p = 85$ kPa, and $q = 30$ kPa. Here, $p = (\sigma_1 + \sigma_2)/2$ is the volumetric stress (or pressure), and $q = \sqrt{(\sigma_2 - \sigma_1)^2 + 2\sigma_{12}^2}$ is the deviatoric stress. σ_1 is the lateral stress, σ_2 is the axial stress, and σ_{12} is the shear stress.

The loading history for assembly 2 involved two stages of loading to match the stress state of the first assembly. First stage was isotropic unloading, and second stage was axial loading at constant lateral stress, resulting in the same p and q as assembly 1. The fabric anisotropy of the second assembly was predominantly vertical, oriented at an angle of 5 degrees counter-clockwise with the vertical. This was very similar to the initial assembly, oriented at an angle of 7 degrees counter-clockwise with the vertical (Figure 4.2). The assembly had a resultant void ratio of $e = 0.15$ (which is very similar to the void ratio of assembly 1).

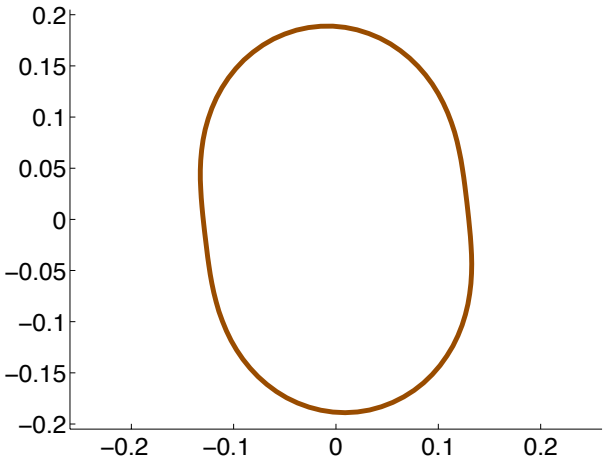

(a)

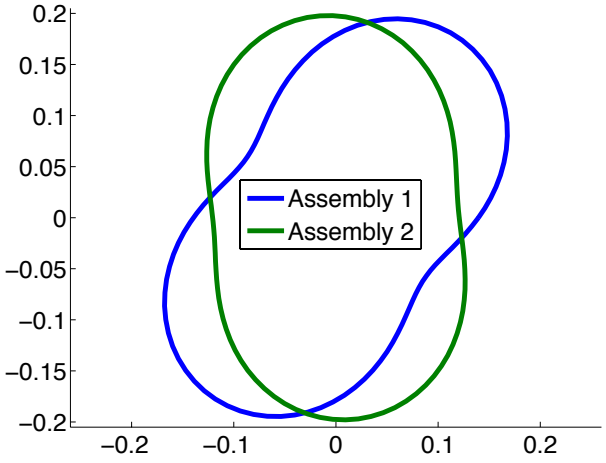

(b)

Figure 4.2: Fabric anisotropies of different assemblies. (a) Initial assembly with A = 0.19, θ_F = -7 degrees. (b) Assembly 1 with A = 0.34, θ_F = 34 degrees, Assembly 2 with A = 0.25, θ_F = -5 degrees. Here A is fabric anisotropy and θ_F is fabric orientation measured clockwise from the vertical, as defined in section 4.2.

4.3 Liquefaction behavior

Liquefaction behavior is associated with undrained, or constant volume loading. Here, the assemblies were subjected to biaxial loading, with axial compression under constant volume constraint. Results are shown in Figure 4.3. Assembly 2, whose fabric anisotropy is largely aligned with the direction of axial compression (vertical) shows stable strain-hardening behavior. However, assembly 1, whose fabric anisotropy is oriented at angle of 34 degrees to the vertical, shows extensive

strain-softening associated with liquefaction behavior. Figure 4.3 clearly demonstrates how two assemblies with the same stress state and void ratio can exhibit different behavior if their fabric is different.

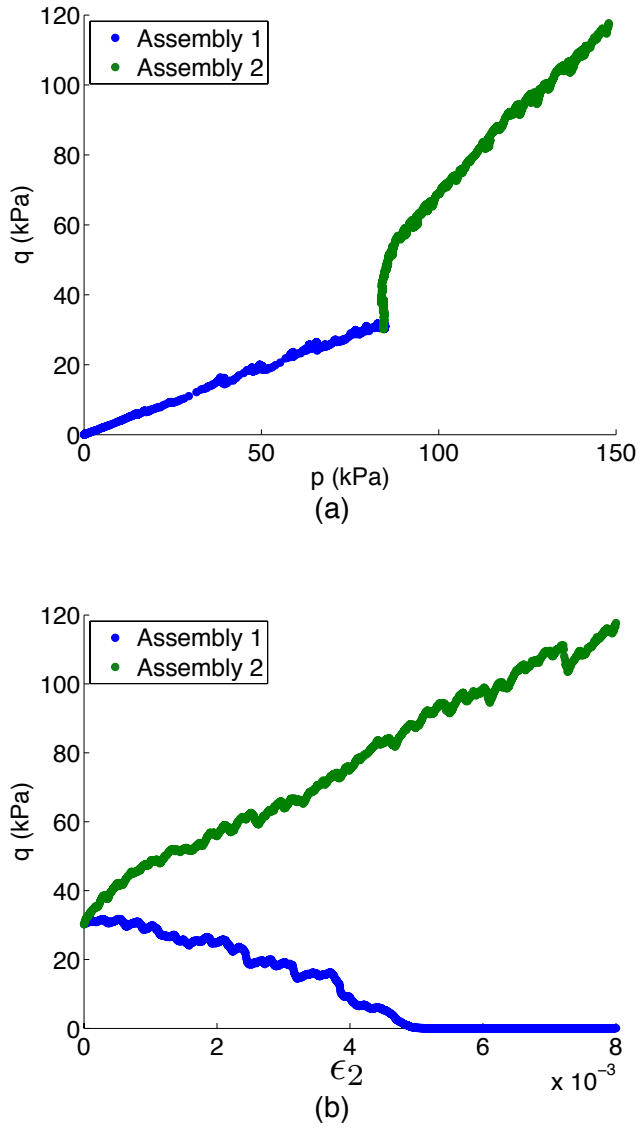

Figure 4.3: Liquefaction behavior results. (a) deviatoric stress (q) vs volumetric stress (p). (b) deviatoric stress (q) vs axial strain (ϵ_2). Assembly 1 exhibits extensive strain-softening associated with liquefaction behavior, whereas assembly 2 shows stable strain-hardening behavior.

The high strength of assembly 2 is expected in light of contact orientations as visualized in Figure 4.2. A high contact anisotropy in the direction of loading facilitates

load transmission through the granular assembly, and makes the assembly more dilatant. [50, 67].

4.4 Shear velocity estimation

Having seen the two assemblies show distinct liquefaction behaviors, we now seek to estimate the small-strain shear velocities of the two assemblies. From the prevalent understanding of V_S-based liquefaction correlations, we expect assembly 2 to have a higher vertical V_S than the assembly 1.

Different approaches exist to estimate the shear velocity or shear modulus of a granular assembly. From a theoretical standpoint, early investigations studied the behavior of two equal spheres pressed together by a normal force and then subjected to a shearing force [56, 57]. Subsequent theoretical investigations considered an aggregate of equal spheres in a cubic packing [23] and in a face-centered cubic lattice [26]. Experiments on a rod of steel spheres [26] demonstrated that shear velocity predictions obtained from theories of perfect spheres can not be expected to agree closely with experiments on real granular soils. Early experimental investigations to study wave propagation in sands involved the 'resonant-column test' [30, 35]. This test subjected a vertical column of sand to longitudinal or torsional oscillations. More recently, an alternate experimental technique called the 'bender element test' [49, 74] was developed. Over the years, the bender element test has gained popularity owing to its simplicity and ease of use, and has also been implemented numerically using the discrete element method [54, 64, 65]. This makes the numerical bender element test an excellent candidate to estimate shear velocities in our granular assemblies.

Numerical bender element test

The bender element test consists of a transmitter element that generates a shear wave, and a receiver element that detects the transmitted disturbance. We chose a bin of particles as the transmitter element. In simulations, as opposed to experiments, it is possible to know the displacement of each particle. Therefore, instead of having a single particle act as a receiver, we tracked the shear displacement for a central column of grains (away from the boundaries) along the entire length of the assembly (denoted by grains colored with a black to white gradient in Figure 4.4). This simplified the analysis as it became convenient to identify shear waves. The assembly was discretized into bins with approximate dimensions 40×40 pixels,

or 4.4×4.4 mm^2. We plotted two-dimensional contours of the central column of particle displacements along the direction of propagation. In the contour plot, the zero crossings of the received signals were clearly visible as a distinct contour line. The average slope of this line was then taken as the shear wave velocity [65]. Figure 4.5 shows the bender element test results for an 800 grain assembly, isotropically consolidated to 50 kPa. The transmitter bin was the bottom-most bin of the central column. The slope of the zero contour line yielded a shear velocity estimate of V_S = 202 m/s.

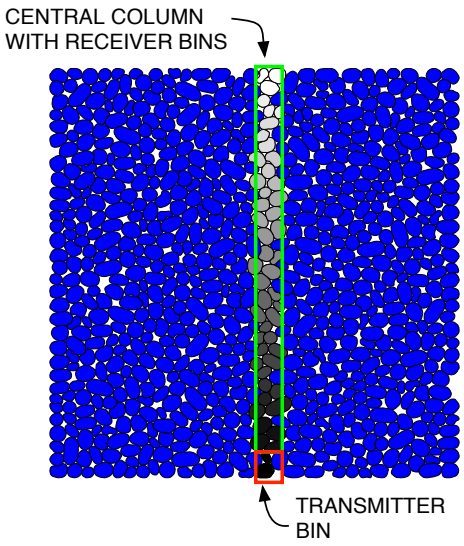

Figure 4.4: Illustration of how shear displacement is tracked for a central column of grains. The central column is denoted by grains that are colored with a black to white gradient.

We used a square wave input with a rise time of 100 time steps and amplitude of 1 pixel. A square wave is a robust input signal that contains all the frequencies [49]. A drawback of the square wave is that the system response necessarily exhibits a 'near-field' effect due to faster moving compressional waves [68]. As a result, it is often not straightforward to determine the arrival of the shear wave. Although the point of first inflection is sometimes considered to be a fair estimate of shear wave arrival [82], research suggests that the arrival of the shear wave does not correspond to a distinctive point in the signal [54]. Various signal interpretation techniques exist to aid in estimating shear wave velocity in an experimental bender element test[65, 87]. For our purpose, since we have access to displacement of each particle, we tracked the shear displacement for a central column of grains along the

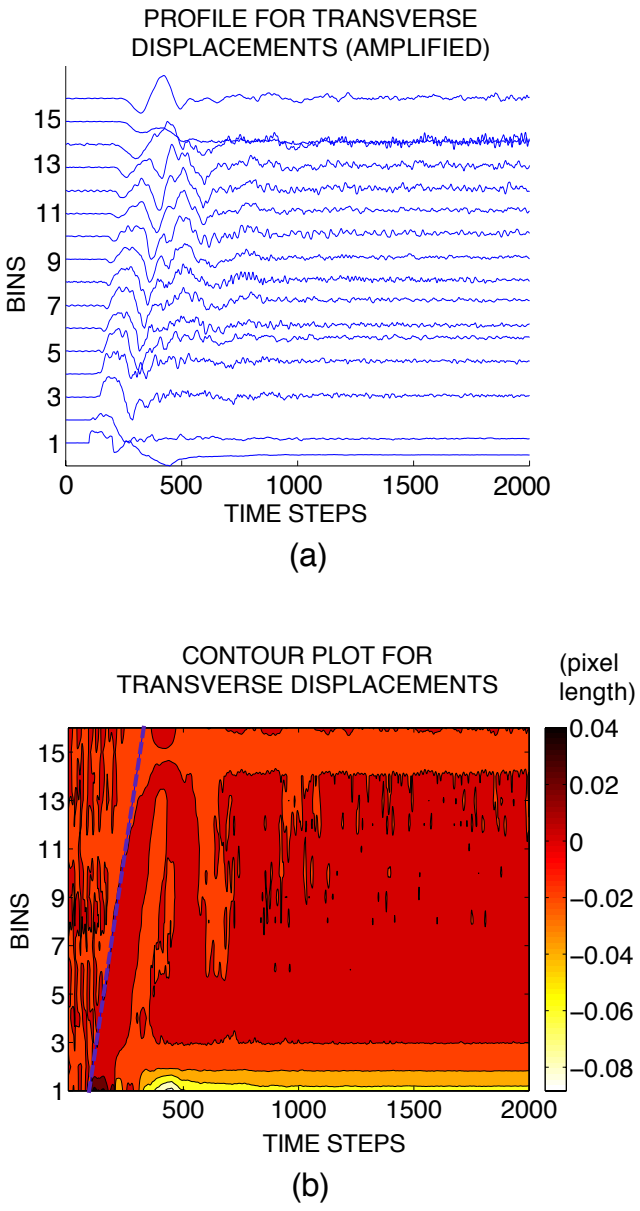

Figure 4.5: Shear velocity estimate for the assembly in Figure 4.4. The blue line in the contour plot in (b) is the average slope estimate for the zero crossing of the received signal, yielding V_S = 202 m/s. 1 bin $\approx 40 \times 40$ pixels, 1 pixel length = 0.1095 mm, 1 time step = 1.36 μs.

entire length of the assembly. Note that the area on the contour plot between the initial noise and the zero contour line corresponds to the near field effect.

Verification exercise

In order to verify our implementation of the bender element test, we also estimated the shear wave velocity V_S by calculating $G_{\max}$ in a biaxial test. The two quantities

are related as:

$$V_S = \sqrt{\frac{G_{\max}}{\rho}} \tag{4.4}$$

where ρ is the density of the granular assembly. To measure $G_{\max}$, an assembly in an isotropic stress state can be subjected to an axial strain of 10^{-4}. This value of strain coincides with the value of 'threshold strain', as defined by Dobry et al [25]. The threshold strain is the strain value till which all the deformations in the granular assembly can be assumed to be elastic. In our 3200 grain assembly, isotropic consolidation also resulted in shear stresses on the walls, typically of the order of about 1% of the confining pressure. Such a small amount of shear stress was sufficient to generate non-linear stress-strain curves, which disabled the approximation of elastic constants. Therefore, we resorted to the smaller 800 grain assembly, prepared as described in section 4.2. When the smaller assembly was consolidated to a pressure of 50 kPa, shear stresses on the wall were negligible ($\sim 0.2\%$ of confining pressure). Axial loading to threshold strain yielded a linear stress-strain curve (Figure 4.6), making it suitable for computing $G_{\max}$, and consequently V_S, enabling a comparison with the V_S estimate obtained in Figure 4.5.

Following the approach by O'Donovan et al [64], we conducted a biaxial stress at constant lateral stress, till an axial strain of 10^{-4} was achieved. As shown in Figure 4.6, the plot of deviator stress q vs axial strain ϵ_2 is a straight line. The slope of the plot, which is within the limit of threshold strain, yields the elastic Young's Modulus E:

$$E = \frac{dq}{d\epsilon_2} = 237 \text{ MPa} \tag{4.5}$$

where dq is the increment in deviatoric stress, and $d\epsilon_2$ is the increment in axial strain. Note that deviatoric stress $q = \sigma_2 - \sigma_1$. Furthermore, by monitoring the lateral strain ϵ_1, we also obtained the poisson's ratio ν, as shown in Figure 4.6:

$$\nu = \frac{-d\epsilon_1}{d\epsilon_2} = 0.21 \tag{4.6}$$

where $d\epsilon_1$ is the increment in lateral strain. $G_{\max}$ was then calculated as:

$$G_{\max} = \frac{E}{2(1+\nu)} = 97.9 \text{ MPa} \tag{4.7}$$

To obtain V_S, we need the density ρ of the granular assembly, which was calculated as:

$$\rho = \frac{\rho_{\text{grains}} \times A_{\text{grains}}}{A_{\text{tot}}} = 2.33 \times 10^3 \text{ kg/m}^3 \tag{4.8}$$

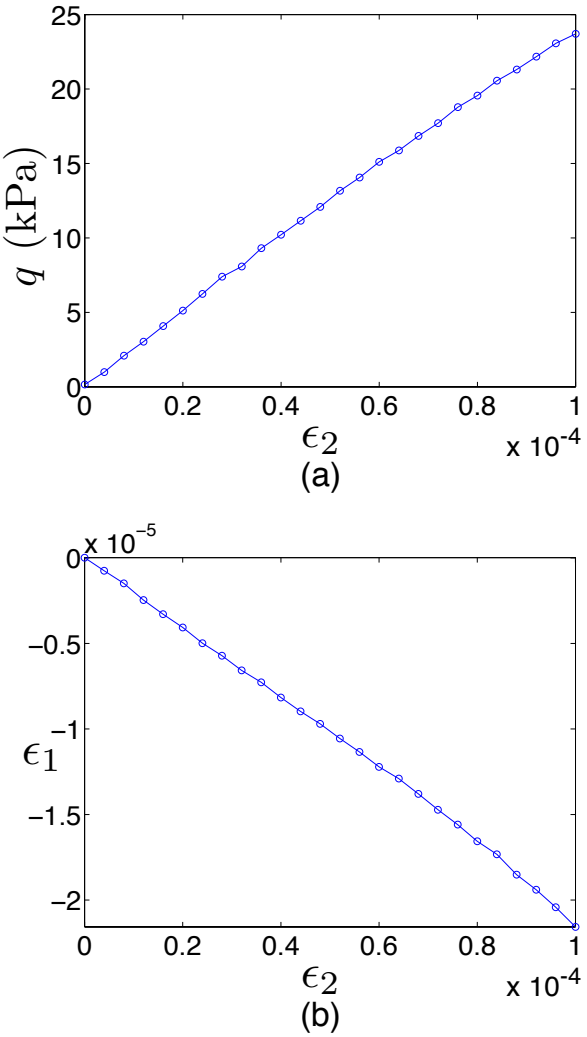

Figure 4.6: Biaxial test at constant lateral stress for the 800 grain assembly, up to an axial strain corresponding to threshold value of 10^{-4}. (a) deviator stress vs axial strain, yielding an elastic Young's modulus of 237 MPa. (b) Lateral strain vs axial strain, yielding a poisson's ratio of 0.21.

where $\rho_{\text{grains}} = 2.7 \times 10^3$ kg/m^3 is the density of grains as specified in Table 4.1, $A_{\text{grains}} = 4.3 \times 10^3$ mm^2 is the total area of grains in the assembly, and $A_{\text{tot}} = 4.99 \times 10^3$ mm^2 is the total area of the assembly. Finally using equation 4.4, the shear velocity was found to be $V_S = 205$ m/s, which is in good agreement with the V_S estimate obtained in Figure 4.5.

Shear Velocity results

Once verified, we used the numerical bender element test technique to obtain V_S estimates for the two 3200 grain assemblies. The assemblies were discretized into

bins with similar dimensions as those specified in Figure 4.5, and the transmitter bin was perturbed horizontally with a square input wave, that had the same rise time and amplitude as in the 800 grain example used for verification. Since V_S is a proxy for liquefaction resistance, it is reasonable to expect that in the vertical direction, assembly 1, which showed extensive strain-softening associated with liquefaction, should have a lower vertical V_S than assembly 2, which exhibited stable strain-hardening behavior. We consider V_S in the vertical direction since that is the direction in which the two assemblies were subjected to axial compression. Subsequently, we also estimate V_S in different directions to investigate the correlation of anisotropy of V_S with the fabric.

Figure 4.7 shows contour plots with average slope estimates, for the 3200 grain assembly 1 and 3200 grain assembly 2. For these plots, the transmitter bin was not the bottom-most bin of the central column. Different locations of the transmitter bin along the central column yielded slightly different V_S estimates, owing to the inherent heterogeneity of the assembly. Therefore, multiple tests (at least three) were simulated with transmitter bins placed at different locations along the central column in order to obtain statistical estimates of V_S.

It is possible that our technique of assembly generation induced significant heterogeneities in the grain fabric. For certain tests, contour plots did not yield distinct contour lines corresponding to zero crossing. Figure 4.8 shows one such test, where there is a high signal dissipation resulting in the lack of a distinct contour line beyond the first few receiver bins. A distinct contour line is necessary in order to estimate its average slope, and consequently V_S. While estimating the slope, we considered a subset of the contour line to ensure that the average slope line (dashed blue line in Figures 4.5 and 4.7) passes the transmitter bin near the time step corresponding to initiation of the input wave.

Table 4.2 shows the test results for V_S in the vertical direction for assemblies 1 and 2, along with the computed mean values. The paucity of results for assembly 1 is due to the fact that a lot of tests produced contour plots similar to those in Figure 4.8, and were unable to yield V_S estimates. The statistics show that on average, estimates of vertical V_S for assembly 2 are higher than those of assembly 1. Table 4.2 clearly shows that the difference in liquefaction resistance of assemblies 1 and

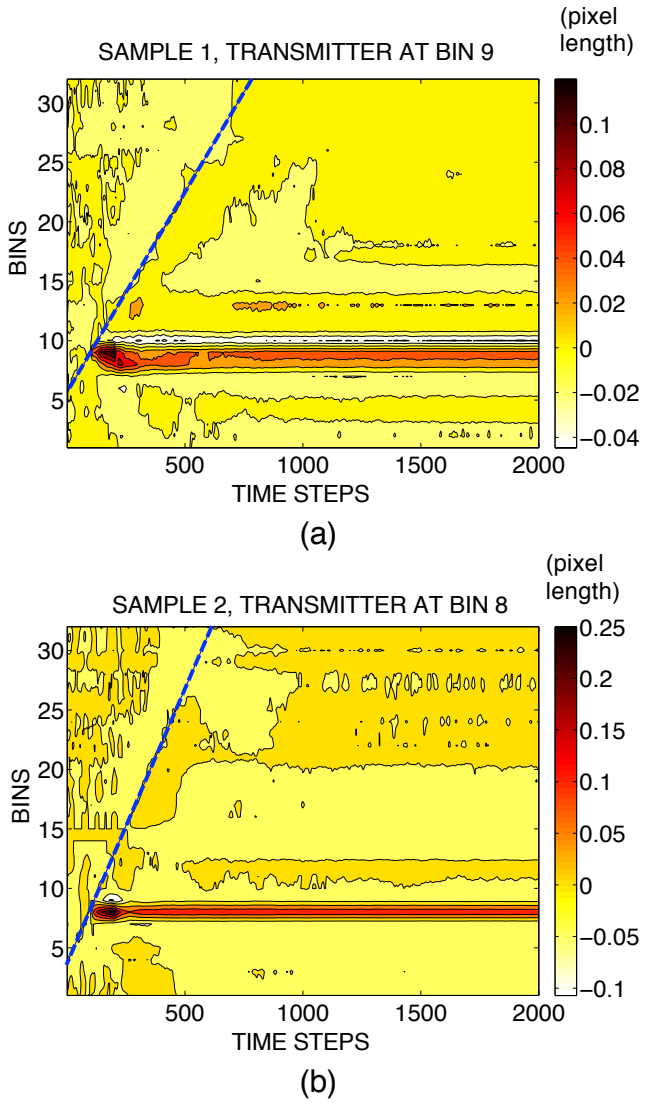

Figure 4.7: Contour plots for transverse displacement. (a) assembly 1. (b) assembly 2. The dashed blue line on the plots is the average slope estimate for the zero crossing of the received signal, which yields a V_S estimate (110 m/s for assembly 1 and 148 m/s for assembly 2). 1 bin $\approx 40 \times 40$ pixels, 1 pixel length = 0.1095 mm, 1 time step = 1.36 μs.

2 (as shown in Figure 4.3), is also accompanied by a difference in their vertical V_S. The assembly that is resistant to liquefaction shows a higher vertical V_S, something that is also expected from the current understanding of V_S-based liquefaction correlations [34, 88].

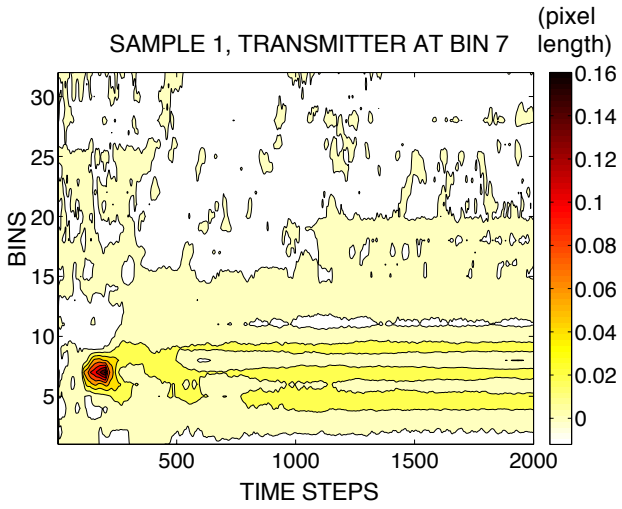

Figure 4.8: Contour plot for transverse displacement, for assembly 1 with transmitter at bin 7. Note the high signal dissipation and the lack of a distinct contour line beyond the first few receiver bins, which disables a V_S estimation. 1 bin $\approx 40 \times 40$ pixels, 1 pixel length = 0.1095 mm, 1 time step = 1.36 μs.

Table 4.2: Test results for V_S in the vertical direction for assemblies 1 and 2

Bin location (Transmitter)	Assembly 1 V_S (m/s)	Assembly 2 V_S (m/s)
1	-	113
2	-	-
3	115	-
4	-	-
5	-	-
6	-	122
7	-	-
8	-	148
9	110	142
10	105	136
11	-	126
Mean	110	131

Correlation of V_S anisotropy with fabric anisotropy

In addition to obtaining estimates for vertical V_S for assemblies 1 and 2, we also obtained estimates for V_S in different directions. This was done to investigate a possible correlation between anisotropy of shear-stiffness or V_S and fabric anisotropy. We conducted an 'angle sweep', i.e., we conducted tests where the transmitter bin was sheared at an angle to the horizontal to transmit a shear wave at an angle.

Figure 4.9 illustrates one such test configuration. The central column (denoted by grains with a black to white gradient) which acted as the receiver was inclined, or rotated, at the same angle with the vertical. Furthermore, the transmitter bin was placed away from the boundaries to prevent wave reflections from corrupting the test results. As observed for vertical V_S estimates, different locations of the transmitter bin along the central column yielded slightly different V_S estimates, owing to the inherent heterogeneity of the assembly. Therefore, multiple tests (at least three) were simulated with the transmitter bin placed at different locations along the central column to obtain statistical estimates of V_S. As with the vertical V_S tests, not all tests yielded contour plots with distinct contour lines corresponding to zero crossing. For the 'angle sweep', the inclination angle θ of the central column was varied from $(-90, 90]$ degrees, in increments of 30 degrees. The angle is positive when measured clockwise from the vertical. This yielded V_S estimates for the entire rotation of 360 degrees since the central column is the same for rotation of θ and $\theta + 90$ (degrees). Figure 4.10 shows the results of the 'angle sweep' for assemblies 1 and 2.

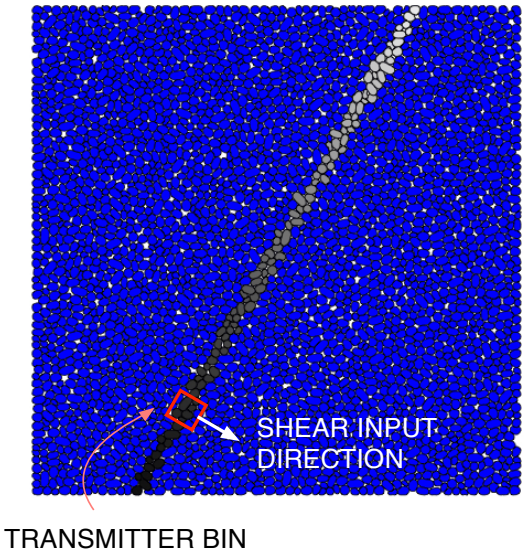

Figure 4.9: Illustration of how V_S estimates are obtained in different directions. The central column (denoted by grains that are colored with a black to white gradient) is rotated at a desired angle with the vertical. The transmitter bin is located in the central column and is sheared perpendicular to the inclination of the central column.

A comparison of anisotropic V_S estimates for assembly 1 (Figure 4.10a) with its fabric anisotropy (Figure 4.2b) suggests a strong influence of contact anisotropy on V_S. Assembly 1 has the majority of contacts aligned at angle of 34 degrees from

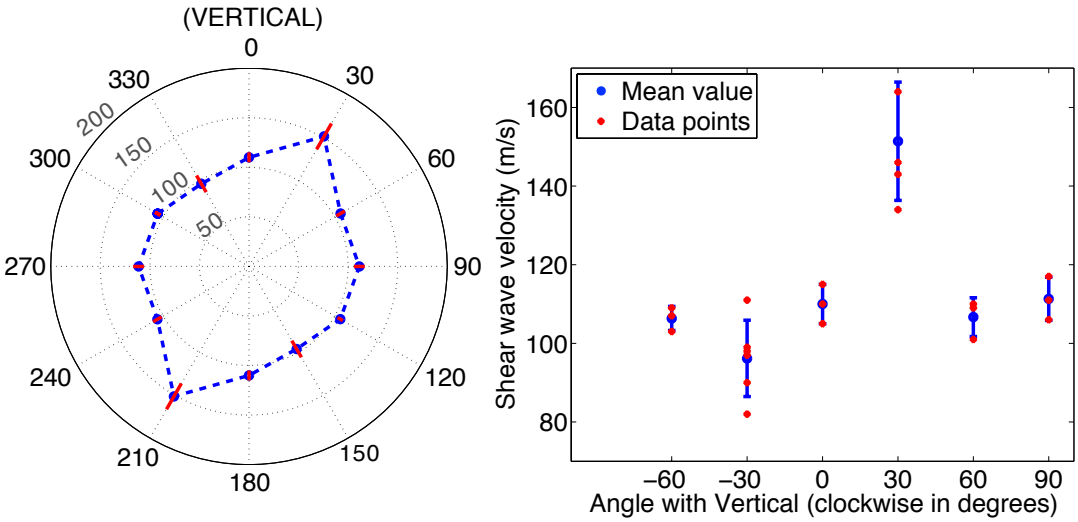

(a) Assembly 1

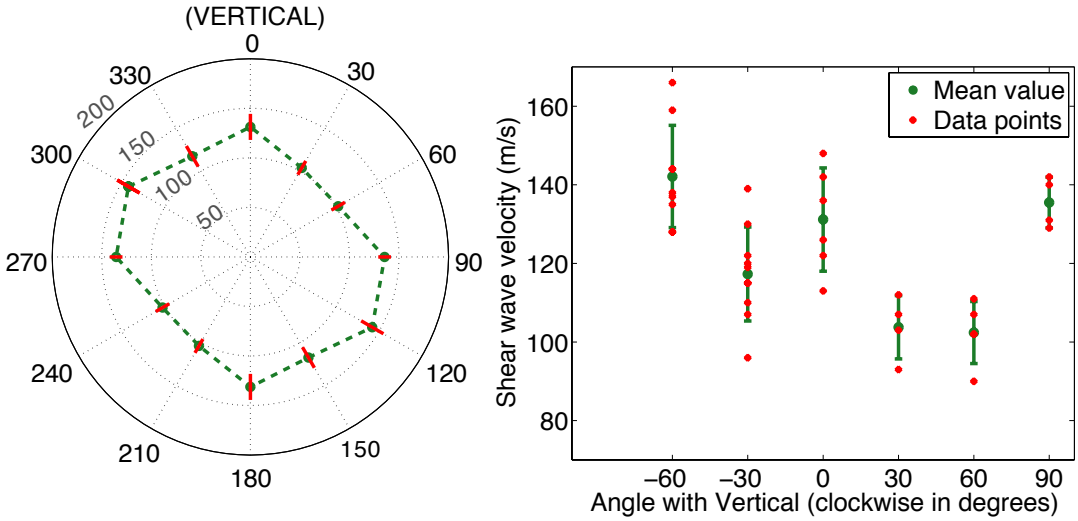

(b) Assembly 2

Figure 4.10: Results of V_S 'angle sweep', giving estimates of V_S in different directions. (a) Assembly 1, (b) Assembly 2. Left: Polar plot with the radius corresponding to V_S, and angle corresponding to angle with vertical (clockwise). Right: Linear plot of V_S vs angle with vertical. The error bars correspond to one standard deviation.

the vertical, and also has the highest V_S in the corresponding orientation, suggesting a strong dependence of shear-stiffness on contact normals. This is not surprising, since the assembly was subjected to simple shear loading (section 4.2), causing the contacts to preferentially align along the principal direction of loading.

The anisotropic V_S estimates for assembly 2 (Figure 4.10b) do not seem to corre-

late well with its fabric anisotropy (Figure 4.2b). There is an anomalous peak in V_S at a direction of 60 degrees counter-clockwise from the vertical. While a detailed investigation of this anomaly is beyond the scope of current work, a cursory investigation suggests a plausible answer. Firstly, it may be noted from Figure 4.2 that while generating assembly 2, the change in fabric from the initial configuration was minimal. Therefore, as opposed to assembly 1, assembly 2 did not experience large-scale destruction and creation of contacts. Secondly, we investigated the fabric anisotropy of increasingly strong contacts. A strong contact is one whose contact force is higher than the mean contact force of the assembly [12]. Interestingly, for the initial assembly, the fabric anisotropy of the ten strongest contacts was largely aligned with the horizontal (Figure 4.11a). Furthermore, the fabric anisotropy of the 10 strongest contacts for assembly 2 was aligned at about 20 degrees counter-clockwise from the vertical (Figure 4.11b). Such anomalous orientation of the strongest contacts was not prevalent in assembly 1 (not shown). This suggests the possibility of assembly 2 having contacts with high compressive forces along the horizontal axis as well as along 60 degrees counter-clockwise from the vertical, which contributed to the high stiffness and consequently high V_S estimates in those directions. Since our fabric quantification did not account for the magnitude of contact forces, the aforementioned contacts were averaged out. It is possible that a more sophisticated fabric estimate that can better capture this effect.

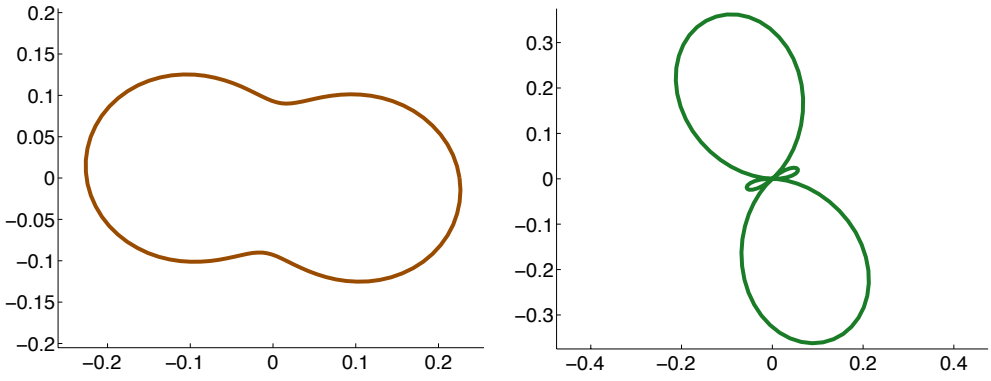

(a) (b)

Figure 4.11: Fabric anisotropies of the ten strongest contacts. (a) Initial assembly with A = 0.43, θ_F = 97 degrees. (b) Assembly 2 with A = 1.38, θ_F = -20 degrees. The small lobe perpendicular to the main lobe is a numerical artifact caused by using the Fourier fit as defined in equation 4.3. Here A is fabric anisotropy and θ_F is fabric orientation measured clockwise from the vertical, as defined in section 4.2.

4.5 Conclusions

Figure 4.3 shows that the two 3200 grain assemblies behave differently under constant volume biaxial compression. Table 4.2 shows that the two assemblies also have different vertical V_S estimates, with the strain-hardening assembly having a higher vertical V_S than the strain-softening assembly. In addition, Figure 4.10 shows that the two assemblies also yield distinct anisotropic estimates of V_S. Although there is some uncertainty in measurements of V_S, the trends are clear. Both assemblies have the same initial stress state characterized by the volumetric stress p, deviatoric stress q, as well as a similar void ratio e. The only difference is fabric, which we quantify on the basis of contact normals. This suggests that while assessing liquefaction potential in the field, V_S might serve as a suitable proxy to estimate not just the prevailing stress state and relative density, but also the prevailing soil fabric. Our results suggest the existence of a correlation between V_S anisotropy and fabric anisotropy—a correlation that can be explored with more detailed micro-mechanical investigations. Such investigations may benefit by the use of periodic boundary conditions. Results of such future investigations could imply that a knowledge of V_S anisotropy in the field would give us insight regarding the micro-mechanical structure of in-situ soil. For lab testing or simulation of soils, this could help in selection or development of a sample preparation technique that yields a similar V_S anisotropy as that in the field. Furthermore, a comparison of in-situ fabric and laboratory fabric could aid researchers in more accurately mapping laboratory or simulation results to field conditions.